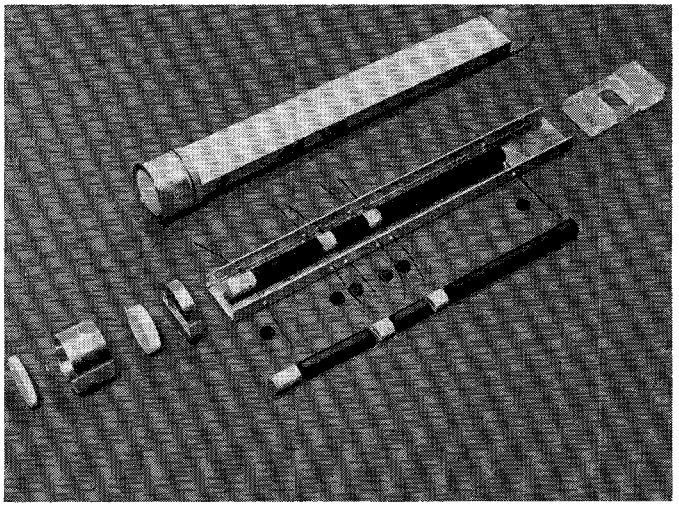

Fig. 6. Developmental array phaser showing feedthroughs.

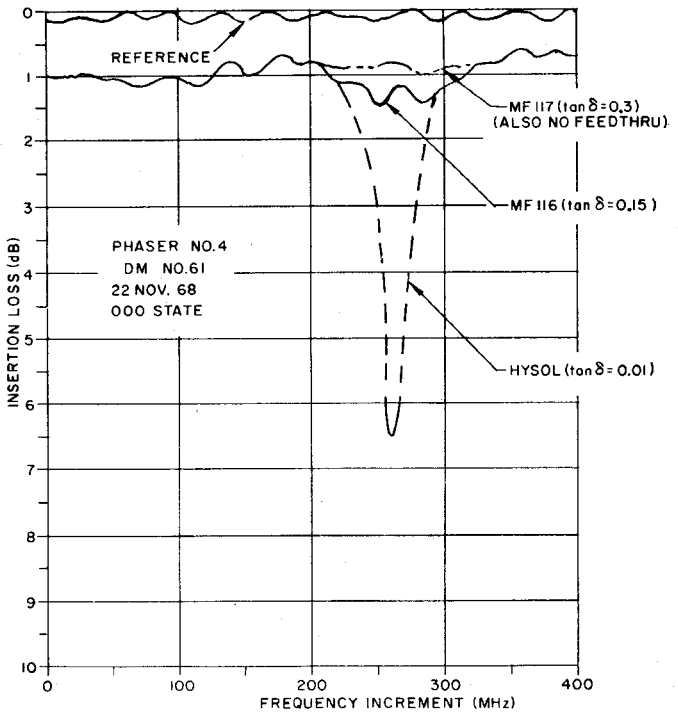

Fig. 7. VSWR versus isolation.

A second group of 15 phasers was fabricated using techniques identical to those used on the initial group of 10 except with improved feedthroughs. The feedthrough material had a dielectric loss tangent of 0.08 and a magnetic loss tangent of about 0.12, making the effective loss tangent about 0.15. Only 3 out of 15 elements exhibited resonances and the average peak absorption in those elements with resonances was 0.5 dB. These results are generally consistent with what would have been predicted from Fig. 5.

In order to compare the resonance reduction capability of several different feedthrough materials, a third experiment was conducted. A swept frequency loss measurement was made on a single phaser, using no feedthroughs and each of three different types of lossy feedthrough. The results from four sets of these measurements are shown in Table I. As an example, the measured insertion loss versus frequency for Phaser 4 is plotted in Fig. 7.

In conclusion, the absorption resonances and RF leakage which have long been associated with digital latching phasers can now be eliminated by a systematic choice of feedthrough material and dimensions. In addition, the feedthrough allows wider ferrite and waveguide assembly tolerances and results in a less expensive device.

TABLE I

LOSSY FEEDTHROUGH COMPARISON
PEAK ABSORPTION-RESONANCE AMPLITUDE (dB)

Type	Tan δ	Phaser 1	Phaser 2	Phaser 3	Phaser 4
1	0.01	8.0	2.8	2.3	5.5
2	0.15	1.5	0.2	0.2	0.6
3	0.3	1.0	0.2	0.2	0.3
None		0.2	0.2	0.2	0.2

REFERENCES

[1] D. H. Temme *et al.*, "A low cost latching ferrite phaser fabrication technique," presented at the 1969 G-MTT Int. Microwave Symp., Dallas, Tex.
[2] N. Marcuvitz, Ed., *Waveguide Handbook* (Radiation Lab. Series 10). Boston, Mass.: Boston Technical Publishers, 1967, pp. 32, 33.
[3] J. Frank, J. Kuck, and C. Shipley, "Latching ferrite phaser shifter for phased arrays," *Microwave J.*, Mar. 1967.

A Dominant Mode Analysis of Microstrip

R. P. WHARTON AND G. P. RODRIGUE

***Abstract*—A computer-aided numerical analysis of the dominant mode propagating in microstrip transmission line is reported, and the theoretical results are corroborated by experimental measurements. A region of almost complete circular polarization is found to exist at the surface of the dielectric, although most of the energy is concentrated directly beneath the strip conductor where the fields possess almost complete linear polarization.**

INTRODUCTION

This analysis of the field distributions in microstrip transmission lines has been carried out in two parts: a theoretical analysis yielding a numerical solution and an experimental study using a small YIG sphere as a field probe. The work was prompted by the knowledge that in order to satisfy all the boundary conditions, the microstrip mode has to be a combination of TE and TM modes existing simultaneously, thus forming a TE–TM hybrid mode. Yet, propagation constant data calculated under a TEM assumption yields good agreement with experimental results. In addition, a laboratory investigation has indicated the existence of a region of circular polarization as evidenced by the realization of a strongly nonreciprocal microstrip resonance isolator [1].

THEORETICAL ANALYSIS AND RESULTS

The theoretical approach [2] used here has been to solve the vector Helmholtz equations numerically for the longitudinal electric and magnetic fields. Since microstrip by its very nature is an open structure, a quantized model would require a subdivision of the region around it into an infinite number of mesh points. Thus it was necessary to enclose the region around the microstrip with a bounding wall. Experimentally, the microstrip fields are found to decay to zero far away from the center strip, thus in this work the longitudinal electric and magnetic fields were required to vanish at those walls. In the microstrip model the dielectric substrate is assumed to be linear, homogeneous, and isotropic. The lossless case is assumed so that the propagating mode is considered to have a z dependence of the form $e^{j(\omega t-\beta z)}$. The strip and ground plane are treated as being infinitely thin and perfectly conducting.

Finite-difference equation representations of the Helmholtz equations were derived for both longitudinal field components. The

Manuscript received August 19, 1971; revised November 5, 1971.
R. P. Wharton is with Schlumberger Well Services, Houston, Tex. 77001.
G. P. Rodrigue is with the School of Electrical Engineering, Georgia Institute of Technology, Atlanta, Ga. 30319.

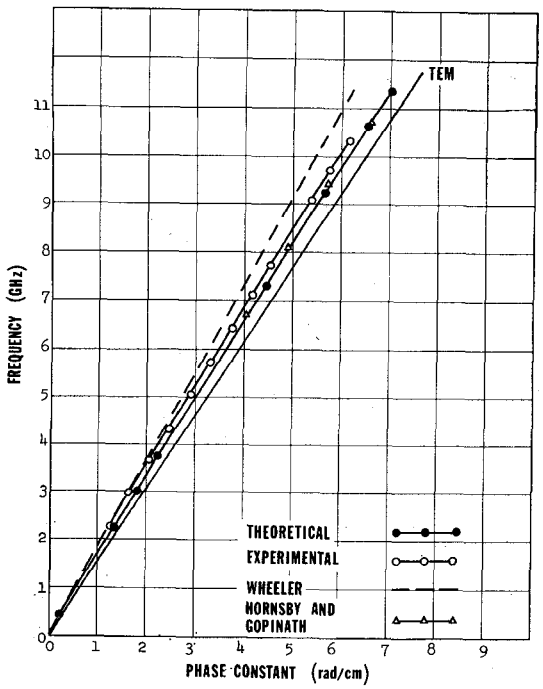

Fig. 1. Experimental and theoretical $f-\beta$ diagrams for the 0.055-in alumina substrate with $w/b=2$.

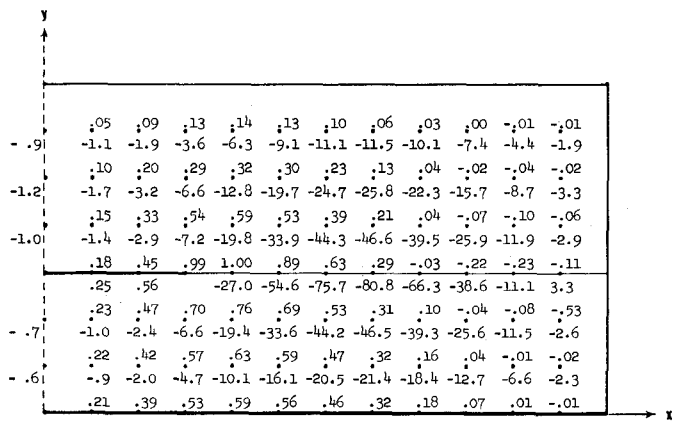

Fig. 2. Longitudinal fields for $\kappa=9.5$, $w/b=2$, and $b=0.055$ in. Magnetic field values are above the node; electric field values are below.

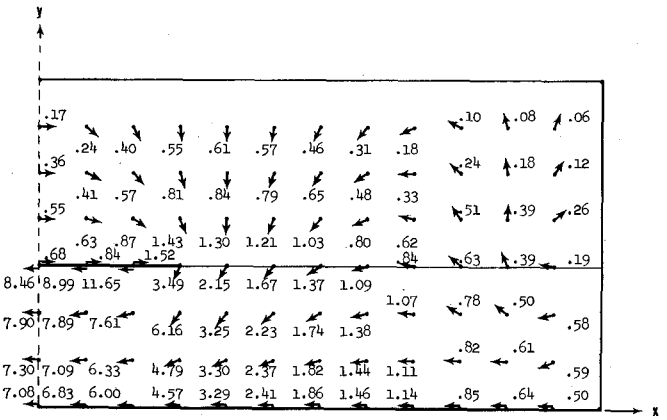

Fig. 3. Transverse magnetic field distribution of the dominant microstrip mode on the 0.055-in alumina substrate at 10.63 GHz.

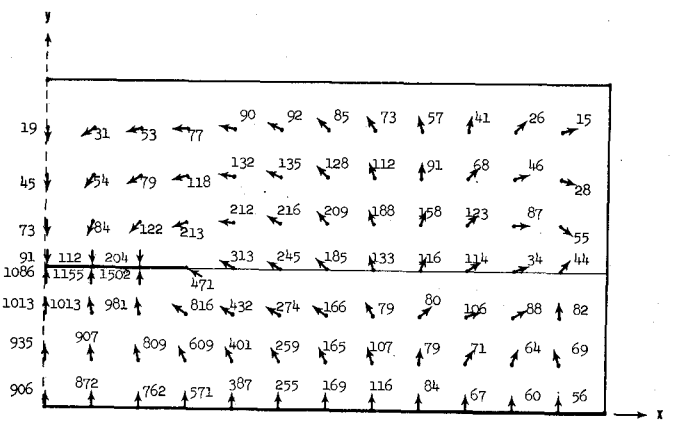

Fig. 4. Transverse electric field distribution of the dominant microstrip mode on the 0.055-in alumina substrate at 10.63 GHz.

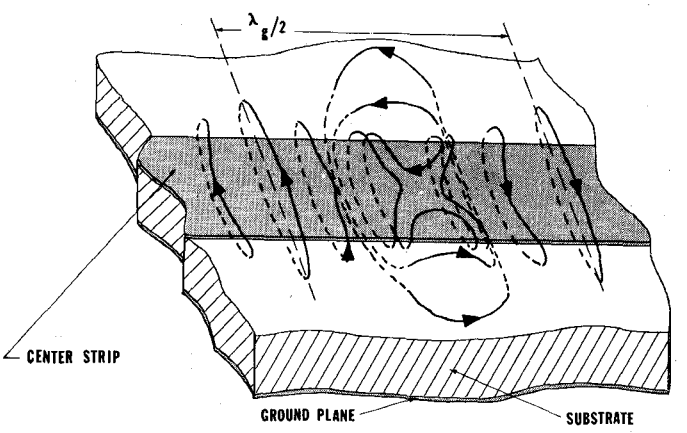

Fig. 5. Magnetic field distribution of the dominant microstrip mode in the vicinity of the center strip.

equations were derived for an unequal spacing of the nodes, thus allowing for their more general placement in the interior of the model configuration. In effect there are two scalar fields superimposed upon each other at each mesh point. These fields are not directly coupled to each other except along regions of discontinuity, in this case the air–dielectric interface. This coupling requires the TE–TM mode superposition to form the hybrid coupled mode.

Two finite-difference equations at each node form a set of linear simultaneous equations which then were cast into an eigensystem form. The eigenvalues were calculated by the QR transformation [3] to yield the phase constant of the propagating mode, and the eigenvectors were calculated via the inverse iteration technique [4] to yield the longitudinal field configurations, both for a given frequency. The transverse field distribution and thus the complete mode pattern were numerically calculated from Maxwell's equations. This approach parallels that of Hornsby and Gopinath [5], but differs in the method of bounding the model and in solving the eigensystem.

The calculated values of phase constant are displayed in Fig. 1 and are compared to those of other investigators [5]–[7]. The straight line labeled TEM corresponds to a TEM mode solution that would propagate if the microstrip were fully loaded with a homogeneous dielectric having a relative permittivity of 9.5. Careful observation of the calculated $f-\beta$ curve reveals that the dominant microstrip mode is slightly dispersive, as also reported by Mittra and Itoh [8].

The calculated longitudinal fields at each node for a 0.055-in alumina substrate ($\epsilon_r=9.5$) with a center strip width to substrate thickness ratio of two are shown in Fig. 2. The transverse fields were calculated from these longitudinal fields and then combined to form transverse field vectors in order to provide a more complete picture of the microstrip mode (Figs. 3 and 4). The magnetic field distribution is shown in Fig. 5; note that this mode has the shape of an inverted saddle.

Experimental Procedures and Results

The phase constants for microwave frequencies between 2 to 12 GHz were determined by loosely coupling RF energy through a microstrip line of known length which had been short circuited at both ends. The shorted line resonated at frequencies for which the line length l was an integral number of guide half-wavelengths $\lambda_g/2$, and from these measurements the experimental $f-\beta$ dispersion curve plotted in Fig. 1 was obtained.

The RF magnetic field components of the microstrip were determined by measuring the relative magnitude of resonance absorption by a YIG sphere used as a probe with the dc field applied along different directions with respect to the transmission line. A ferrimagnetic material can be characterized by a tensor permeability which can be reduced to a scalar form by assuming that the sample is excited by a uniform RF magnetic field polarized either clockwise (CW) or counterclockwise (CCW) in a plane normal to the dc magnetic field. The scalar quantities $(\mu+k)$ and $(\mu-k)$ are the effective permeabilities for these two waves for the lossless case:

$$\mu + k = \mu_0 + \frac{\mu_0 \omega_M}{\omega_0 - \omega}$$

$$\mu - k = \mu_0 + \frac{\mu_0 \omega_M}{\omega_0 + \omega}. \tag{1}$$

When magnetic losses are included, the resonance absorption is finite rather than infinite. Thus the CCW fields exhibit no resonance loss due to spin coupling effects, whereas the CW fields show a strong resonance absorption.

An elliptically polarized RF magnetic field can be resolved into two circularly polarized fields: one CW and the other CCW about a normal to the plane of the polarization. The amplitudes of these circularly polarized fields are easily shown to be of the form $\|h_x/2| \pm |h_y/2\|$ and $\|h_x/2| \pm |h_x/2\|$ where h_x, h_y, and h_z are the component amplitudes of the elliptically polarized field.

The connection between the power absorbed and the RF driving field is found by considering the term $\vec{H}\cdot(\partial B / \partial t)$, which represents a power density in the complex Poynting theorem. The rate of change of stored energy in a unit volume is proportional to $\int_v \overleftrightarrow{\mu} |\vec{H}|^2\, dv$, and the power absorbed per unit volume (UV) is

$$P/\mathrm{UV} \propto \overleftrightarrow{\mu} |\vec{H}|^2. \tag{2}$$

In terms of the circularly polarized fields, this becomes

$$P/\mathrm{UV} \propto \overleftrightarrow{\mu}(|\vec{H}_{\mathrm{CW}}|^2 + |\vec{H}_{\mathrm{CCW}}|^2) + \overleftrightarrow{\mu}(\vec{H}_{\mathrm{CW}}\cdot\vec{H}_{\mathrm{CCW}}^* + \vec{H}_{\mathrm{CCW}}\cdot\vec{H}_{\mathrm{CW}}^*). \tag{3}$$

The second term of this equation can be shown to be zero. In terms of the effective scalar permeabilities, (3) becomes

$$P/\mathrm{UV} \propto \left(\mu_0 + \frac{\mu_0\omega_M}{\omega_0 - \omega}\right) |\vec{H}_{\mathrm{CW}}|^2 + \left(\mu_0 + \frac{\mu_0\omega_M}{\omega_0 + \omega}\right) |\vec{H}_{\mathrm{CCW}}|^2. \tag{4}$$

As the RF frequency is varied through ω_0, the first term will have a zero in the denominator and will exhibit a resonance, whereas the second term will experience a negligible change. The size of the YIG sphere remains constant so, as a result, at a resonance the power absorbed by the sample is proportional to the square of the magnitude of the CW circularly polarized component of the magnetic field:

$$P_{\mathrm{absorbed}} \propto |H_{\mathrm{CW}}|^2. \tag{5}$$

The power absorbed at resonance was not measured directly. Instead, the ratio in decibels of the "at resonance" and the "off resonance" power levels transmitted through the section were measured:

$$\text{absorption in dB} = 10 \log \left(\frac{\text{power}_{\text{off resonance}}}{\text{power}_{\text{off resonance}} - \text{power}_{\text{absorbed}}}\right). \tag{6}$$

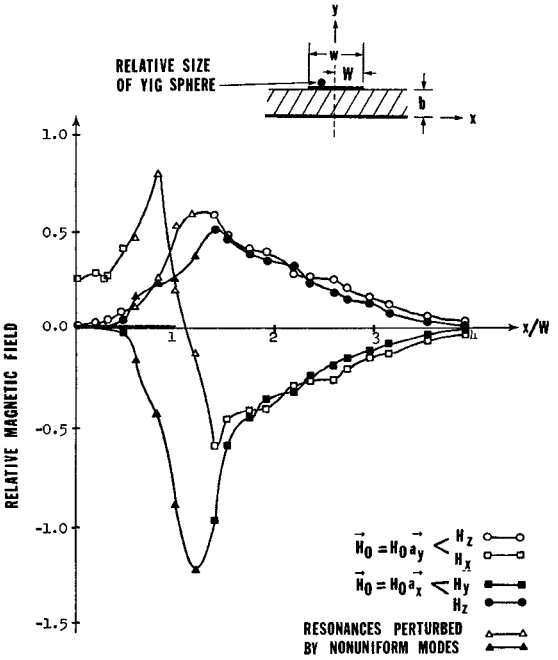

Fig. 6. Magnetic field components calculated from the measured spin resonance absorptions for the 0.055-in alumina substrate with $w/b = 2$ at 10.6 GHz.

The power level into the microstrip was kept constant so that

$$\text{power}_{\text{absorbed}} \propto 1 - \frac{1}{\text{antilog}\left(\dfrac{\text{absorption in dB}}{10}\right)}. \tag{7}$$

Using (5), the amount of resonance absorption is related to the CW circularly polarized component of the magnetic field:

$$|H_{\mathrm{CW}}| \propto \left[1 - \frac{1}{\text{antilog}\left(\dfrac{\text{absorption in dB}}{10}\right)}\right]^{1/2}. \tag{8}$$

In taking these measurements, the RF power level was kept well below 1 mW, otherwise a large resonant absorption could cause heating of the YIG sphere, resulting in a decrease in the saturation magnetization and a decrease in the "on resonance" permeability. To insure that the YIG sphere only weakly perturbed the field distribution, a small diameter (0.0164 in) was used.

The magnetic field components which were calculated from the spin resonance absorption data are plotted in Fig. 6. Note that two H_z curves are plotted, one for each of the two antiparallel orientations of the biasing field. Also shown in Fig. 6 is a cross-sectional view of the microstrip drawn to approximate scale. The large dot represents the relative size of the YIG sphere in relation to the microstrip line. The triangles on the plot indicate the regions on the substrate where nonuniform modes [9] perturbed the uniform mode of resonance absorption. At those regions, coupling to nonuniform modes resulted in a broadening of the resonance line of the principal mode of resonance absorption, and consequently a reduction in the peak resonance absorption curve. The fields calculated at these locations are based on the resonances which were judged to be the uniform mode, but which were probably reduced in amplitude due to coupling to the nonuniform modes.

The theoretically calculated magnetic field components are presented for comparison in Fig. 7. Since the YIG sphere diameter was approximately equal to the node spacing for the 0.055-in substrate, the plotted fields are averages of the field values at the nodes on the interface and the field values at the nodes just above the interface. Comparison of the experimental and theoretical curves in the vicinity of the center strip shows very good agreement. The longitudinal

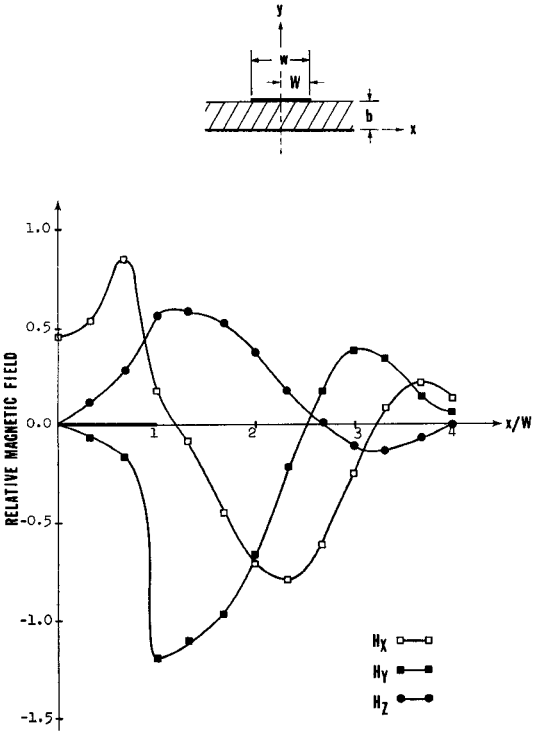

Fig. 7. Relative amplitudes of the numerically calculated magnetic field components for the 0.055-in alumina substrate with $w/b = 2$ at 10.63 GHz.

magnetic field reaches its maximum just past the center strip edge. The x component of the magnetic field reaches its positive extremum just inside the center strip edge, passes through zero just past the edge, and then passes through a negative extremum a short distance from the edge. The y component of the magnetic field drops off zero just past the center strip edge. Note that the longitudinal magnetic field and consequently the longitudinal electric field of the microstrip mode along the interface are far from being negligible quantities.

At regions on the air–dielectric interface in the vicinity of the center strip edge, both the experimental plot (Fig. 6) and the theoretical plot (Fig. 7) reveal a relatively large component of circularly polarized RF magnetic field in planes normal to both the x and y axes. Experimental work by other investigators [1] had indicated that there was a circularly polarized component of the RF magnetic field in microstrip, but its relative location and amplitude were not known.

The only other reported experimental investigation for the field configuration was by Shafer [10]. He used a loop coupling technique to measure the average RF magnetic field distribution on an oversized microstrip line having a low dielectric constant substrate.

Conclusion

The fact that there is a substantial component of longitudinal magnetic field has been demonstrated both experimentally and theoretically. The experimental results corroborated the numerical findings and showed that the dominant propagating mode in microstrip is dispersive and is in fact a hybrid coupled TE–TM saddle mode. At low microwave frequencies, where the guide wavelength becomes much greater than the substrate thickness, the mode begins to approach a TEM mode. It was also shown that substantial amounts of circular polarization of the RF magnetic field exist in each of two orthogonal planes. It should be pointed out, however, that most of the energy in the microstrip mode is concentrated in the dielectric substrate under the center strip, and in this region the longitudinal fields are relatively weak. Consequently, one would expect TEM calculations of guide wavelength, phase constant, etc., to be reasonably close to the actual values.

References

[1] G. R. Harrison, G. H. Robinson, B. R. Savage, and D. R. Taft, "Ferrimagnetic parts for microwave integrated circuits," *IEEE Trans. Microwave Theory Tech., (Special Issue on Microwave Integrated Circuits)*, vol. MTT-19, pp. 577–588, July 1971.
[2] R. P. Wharton, "A dominant mode analysis of microwave hybrid integrated circuit transmission lines," Ph.D. dissertation, Georgia Inst. Technol., Atlanta, Ga., June 1970.
[3] J. G. F. Francis, "The QR transformation, a unitary analogue to the LR transformation—Part 1 and Part 2," *Comput. J.*, vol. 4, pp. 265–271, 332–345, Oct. 1961.
[4] J. H. Wilkinson, *The Algebraic Eigenvalue Problem.* London, England: Oxford Univ. Press, 1965, pp. 321–325.
[5] J. S. Hornsby and A. Gopinath, "Numerical analysis of a dielectric-loaded waveguide with a microstrip line—Finite-difference methods," *IEEE Trans. Microwave Theory Tech.*, vol. MTT-17, pp. 684–690, Sept. 1969.
[6] H. A. Wheeler, "Transmission-line properties of parallel wide strips by a conformal-mapping approximation," *IEEE Trans. Microwave Theory Tech.*, vol. MTT-12, pp. 280–290, May 1964.
[7] ——, "Transmission-line properties of parallel strips separated by a dielectric sheet," *IEEE Trans. Microwave Theory Tech.*, vol. MTT-13, pp. 172–185, Mar. 1965.
[8] R. Mittra and T. Itoh, "A new technique for the analysis of the dispersion characteristics of microstrip lines," *IEEE Trans. Microwave Theory Tech.*, vol. MTT-19, pp. 47–56, Jan. 1971.
[9] B. Lax and K. J. Button, *Microwave Ferrites and Ferrimagnetics.* New York: McGraw-Hill, 1962, pp. 180–189.
[10] C. G. Shafer, "Dominant mode of the microstrip transmission line," Cruft Lab., Harvard Univ., Cambridge, Mass., Contract Nonr-1886(26), Tech. Rep. 257, Nov. 1957.

Octave-Band Microstrip DC Blocks

DAVID LACOMBE AND JEROME COHEN

***Abstract*—The design of octave-bandwidth microstrip interdigital dc blocks is presented. Data for a 7.75- to 16.3-GHz design are given and correlated with an approximate equivalent circuit based on even and odd mode propagation in coupled microstrip. Additional data are tabulated reflecting the ability to shift the frequency band of operation.**

DC blocking capacitors are an important element in the design of several microwave components requiring dc-biased devices. In microstrip, chip and beamlead capacitors, as well as directly deposited thick- or thin-film capacitors, are extensively employed, but each has certain disadvantages. Chip and deposited capacitors are attractive at lower microwave frequencies [1], [2] typically through S band, although reported on as high as X band [3]. In these frequency ranges, they can be considered "lumped-element" components, but become distributed elements and sometimes introduce unwanted parasitics in higher frequency bands. Beamlead devices reduce these problems at high frequencies but are relatively expensive and more difficult to handle, requiring the use of microscopes and sophisticated bonding equipment for installation.

This short paper describes an empirical extension of the interdigital-type dc block reported on by Stinehelfer [4] which has the advantage of being "printed" simultaneously with other microstrip circuitry. The basic circuit, illustrated in Fig. 1, consists of a single

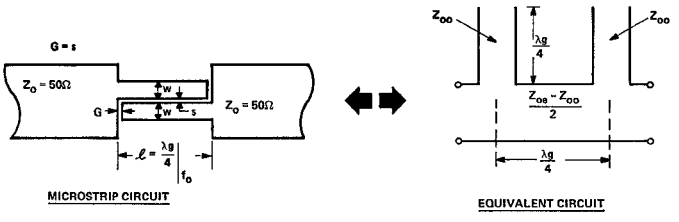

Fig. 1. DC block microstrip circuit and equivalent circuit.

Manuscript received September 7, 1971; revised October 13, 1971. The initial development of this work was conducted in the former Microwave Products group of Monsanto, St. Louis, Mo., now a part of Microwave Associates, Burlington, Mass. The remainder of the work was sponsored by Applied Technology, A Division of Itek Corporation, Sunnyvale, Calif.

D. LaCombe is with the Microwave Integrated Circuit Laboratory, Applied Technology, A Division of Itek Corporation, Sunnyvale, Calif.
J. Cohen is with the Laser-Link Corporation, Woodbury, N. Y.